

# Journal Pre-proofs

Method article

Guided extraction of genome-scale metabolic models for the integration and analysis of omics data

Andrew Walakira, Damjana Rozman, Tadeja Režen, Miha Mraz, Miha Moškon

PII: S2001-0370(21)00247-6  
DOI: <https://doi.org/10.1016/j.csbj.2021.06.009>  
Reference: CSBJ 1063

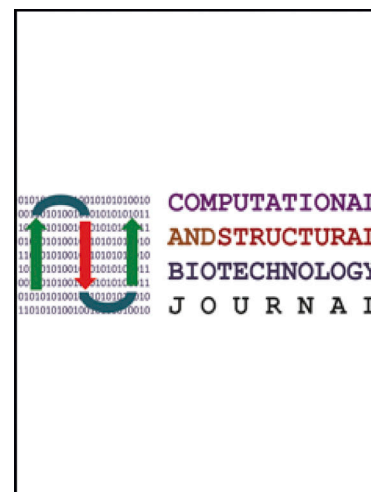
To appear in: *Computational and Structural Biotechnology Journal*

Received Date: 8 April 2021  
Accepted Date: 4 June 2021

Please cite this article as: A. Walakira, D. Rozman, T. Režen, M. Mraz, M. Moškon, Guided extraction of genome-scale metabolic models for the integration and analysis of omics data, *Computational and Structural Biotechnology Journal* (2021), doi: <https://doi.org/10.1016/j.csbj.2021.06.009>

This is a PDF file of an article that has undergone enhancements after acceptance, such as the addition of a cover page and metadata, and formatting for readability, but it is not yet the definitive version of record. This version will undergo additional copyediting, typesetting and review before it is published in its final form, but we are providing this version to give early visibility of the article. Please note that, during the production process, errors may be discovered which could affect the content, and all legal disclaimers that apply to the journal pertain.

© 2021 Published by Elsevier B.V. on behalf of Research Network of Computational and Structural Biotechnology.



1 Guided extraction of genome-scale metabolic models  
2 for the integration and analysis of omics data

3 Andrew Walakira<sup>a</sup>, Damjana Rozman<sup>a</sup>, Tadeja Režen<sup>a</sup>, Miha Mraz<sup>b</sup>, Miha  
4 Moškon<sup>b,c</sup>,

5 <sup>a</sup>*Centre for Functional Genomics and Bio-Chips, Institute for Biochemistry and  
6 Molecular Genetics, Faculty of Medicine, University of Ljubljana, Ljubljana,*

7 <sup>b</sup>*Faculty of Computer and Information Science, University of Ljubljana, Ljubljana,  
8 Slovenia,*

9 <sup>c</sup>*Corresponding author: Miha.Moskon@fri.uni-lj.si*

---

10 **Abstract**

11 Omics data can be integrated into a reference model using various model  
12 extraction methods (MEMs) to yield context-specific genome-scale metabolic  
13 models (GEMs). How to chose the appropriate MEM, thresholding rule and  
14 threshold remains a challenge.

15 We integrated mouse transcriptomic data from a *Cyp51* knockout mice  
16 diet experiment (GSE58271) using five MEMs (GIMME, iMAT, FASTCORE,  
17 INIT and tINIT) in a combination with a recently published mouse GEM  
18 iMM1865. Except for INIT and tINIT, the size of extracted models varied  
19 with the MEM used (t-test: p-value < 0.001). The Jaccard index of iMAT  
20 models ranged from 0.27 to 1.0. Out of the three factors under study in the  
21 experiment (diet, gender and genotype), gender explained most of the vari-  
22 ability (> 90%) in PC1 for FASTCORE. In iMAT, each of the three factors  
23 explained less than 40% of the variability within PC1, PC2 and PC3. Among  
24 all the MEMs, FASTCORE captured the most of the true variability in the  
25 data by clustering samples by gender.

26 Our results show that for the efficient use of MEMs in the context of omics  
27 data integration and analysis, one should apply various MEMs, thresholding  
28 rules, and thresholding values to select the MEM and its configuration that  
29 best captures the true variability in the data. This selection can be guided by  
30 the methodology as proposed and used in this paper. Moreover, we describe  
31 certain approaches that can be used to analyse the results obtained with the  
32 selected MEM and to put these results in a biological context.

33 *Keywords:* genome-scale metabolic model, model extraction methods,  
34 context-specific metabolic model, omics data integration, subsystem  
35 enrichment analysis, model interpretability

---

## 36 1. Introduction

37 The advent of high-throughput technologies generate large volumes of  
38 omics data hence making it possible to study organisms at the cellular level.  
39 These studies have enabled a better understanding of the underlying biologi-  
40 cal processes of many diseases such as diabetes [1, 2] and asthma [3], yielded  
41 useful products such as insulin [4, 5] and antibiotics [6, 7], and also improved  
42 production of commercial products such as wines [8]. However, there is still  
43 a big knowledge gap in the finer details of how organisms, unicellular or mul-  
44 ticellular, are able to maintain life and how disruptions at the molecular level  
45 affect their phenotypes.

46 The phenotypic characteristics of an organism are determined by intri-  
47 cately connected reactions and consequently pathways that generate energy  
48 and other forms of biological products necessary to sustain life and organ-  
49 ise organismal development. These pathways are connected to form and  
50 function as biological systems and thus it is vital to study organisms at  
51 system level. The degree of complexity of biological systems differs greatly  
52 among organisms, for example, humans are far more complex than *Drosophila*  
53 *melanogaster* despite the latter's importance in modelling human diseases  
54 [9, 10, 11]. It is extremely difficult, or even impossible for higher level or-  
55 ganisms, to study the entirety of their pathways either *in vitro* or *in vivo*.  
56 However, mathematical tools such as genome-scale models can be used to  
57 gain insight into how these biological systems function [12].

58 Genome-scale metabolic models (GEMs) are increasingly becoming a pop-  
59 ular tool for studying biological processes *in silico*[13, 14, 15]. GEMs are  
60 formulated to contain all known biochemical reactions involved in maintain-  
61 ing the living state of a cell or an organism (metabolism). Context-specific  
62 metabolic models (also known as tissue-specific models) are GEMs in which  
63 inactive reactions for a given condition (context) are removed [16] and thus  
64 represent the context better since not all possible reactions are active in dif-  
65 ferent cell types and/or in different contexts. Moreover, GEMs can be used  
66 to perform *in silico* studies and observe the dynamical response of the sys-  
67 tem in a given condition using computer simulations. As such, they provide

68 better understanding of the organism as a functional system. One of the  
69 main problems of using GEMs in a combination with omics data lies in the  
70 complexity of the obtained models and the number of models produced. The  
71 obtained results are thus difficult to interpret in the context of biology. More-  
72 over, it is hard to select an appropriate model extraction method (MEM) for  
73 a specific dataset. When the appropriate MEM is selected, it also needs to  
74 be configured, e.g., gene activity thresholds and thresholding rules need to  
75 be defined [17, 18] to yield accurate and biologically relevant results.

76 We aim to address these problems by suggesting a methodology for per-  
77 forming analyses of omics data using GEMs in combination with different  
78 MEMs. This methodology will serve as an essential step towards the de-  
79 velopment of a pipeline that will automatically select a suitable MEM for a  
80 specific dataset, perform its configuration, and extract the models. More-  
81 over, such a pipeline could provide its users with a set of publication-ready  
82 figures and tables, describing the results of simulations performed upon the  
83 derived models as well as the results of different statistical and enrichment  
84 analyses ready for a straightforward interpretation.

## 85 2. Materials and Methods

86 In this section, we describe how a GEM is reconstructed from available  
87 biological information to produce a reference model. This is followed by a  
88 summary of the data integration algorithms that were applied in our analysis.  
89 Finally, we describe our analysis of the dataset used in our case study, namely,  
90 mouse diet experiment data.

### 91 2.1. Genome-scale metabolic models: from reconstruction to simulation

92 The construction of GEMs can be summarised in four main steps as de-  
93 scribed by Feist and colleagues [19]. First, a draft reconstruction of the  
94 biological network of an organism is extracted using information about re-  
95 actions, enzymes, and pathways from databases such as KEGG, BRENDA,  
96 etc. The second step is the manual curation of the reconstructed draft model.  
97 This involves checking and filling the gaps and correcting misplaced reactions.  
98 Here, organism-specific databases and literature are used. Computational al-  
99 gorithms such as GAUGE [20], FastGapFill [21], and FBA-Gap [22] can also  
100 be applied. The third step is the conversion of the reconstructed model into  
101 a mathematical representation that can be used for subsequent simulations.  
102 The final step is the refining, validation, and application of the model to

103 inform decisions. Here, the model outputs are compared with known infor-  
 104 mation to confirm consistency. Model validation can be done by testing how  
 105 well a model performs a set of tasks, comparing the simulation results with  
 106 experimental data for a particular objective such as growth and use of gene  
 107 essentiality analysis i.e. identification of genes that are required for survival  
 108 of an organism [23].

The most efficient approach for prediction of phenotype from genotype using GEMs is constraint-based modelling [24, 25]. Here, it is common to assume that the system is in a steady state, i.e., the concentrations of all metabolites involved are constant (see Equation 1). Constraint-based modelling is focused on predicting flux distributions while optimising a selected cellular function (or a set of functions). Flux Balance Analysis (FBA) is the most widely used technique to predict flux distributions in GEMs [26, 27]. It requires a mathematical representation of the model in the form of a stoichiometric matrix  $\mathbf{S}$  with rows representing metabolites and columns representing reactions. We can evaluate a vector  $\mathbf{v}$  of fluxes through the observed metabolic reactions constrained by the upper and lower flux bounds by using the equation

$$\sum_{j=1}^N S_{ij} \cdot v_j = 0,$$

$$\forall i \in \{1, 2, \dots, M\},$$

$$\forall j \in \{1, 2, \dots, N\},$$

109 where  $M$  is the number of observed metabolites and  $N$  the number of ob-  
 110 served reactions. FBA reduces the problem to a linear program, hence lower-  
 111 ing the computational requirements involved [26]. However, there are certain  
 112 limitations. First, FBA does not yield a unique solution and is highly de-  
 113 pendent on the choice of the objective function, i.e., a description of the  
 114 phenotype relevant to the problem being studied [28]. While in some cases  
 115 biomass optimisation is a plausible biological objective (e.g., cancer cells, cell  
 116 lines, single cell organisms), different optimisation criteria need to be applied  
 117 depending on the question of interest. How to select an appropriate objective  
 118 function is an unanswered question. Algorithms that can select the objec-  
 119 tive function automatically have been proposed [29]. There is also increasing  
 120 evidence that multiple objective functions are required to allow metabolic  
 121 flexibility and improve accuracy of the model [30, 31]. The other challenges  
 122 are that FBA is dependent on the choice of the solver (used to solve the set

123 of linear equations) and the quality of reconstruction [27, 32]. Variations of  
124 FBA have been proposed to ease these limitations for example, parsimonious  
125 FBA (pFBA) [33] and Flux Variability Analysis (FVA) [34], among others  
126 [27, 35]. Another method for predicting metabolic fluxes is flux sampling,  
127 which can be used to estimate probability distributions of reaction fluxes  
128 without assuming any particular cellular objective [36, 37].

## 129 2.2. Computational approaches for experimental data integration

130 Model extraction methods can be classified as members of a "GIMME-  
131 like" family which minimises flux through reactions associated with low gene  
132 expression, an "iMAT-like" family which finds an optimal trade-off between  
133 keeping reactions whose genes are highly expressed and removing reactions  
134 associated with low gene expression, and an "MBA-like" family which retains  
135 a selected set of core reactions [16, 38]. Below is a summary of the data  
136 integration algorithms that were used in this analysis.

### 137 2.2.1. GIMME

138 Gene Inactivity Moderated by Metabolism and Expression (GIMME) [16,  
139 39, 40] uses gene expression data and one or more objective functions to  
140 produce a context-specific model. The GIMME algorithm takes three inputs,  
141 i.e., expression data, genome scale reconstruction, and one or more required  
142 metabolic functionalities (RMFs) that the cell is expected to achieve. The  
143 algorithm first finds a flux distribution that optimises the given objective(s)  
144 and then minimises the use of inactive reactions (reactions whose expression  
145 is below a predefined threshold). The expression data is used directly as  
146 weights in the objective function. A threshold is used to determine if a  
147 weight in the objective is positive or negative. A weight of zero is assigned to  
148 reactions without expression data. The method yields an inconsistency score  
149 i.e. ( $flux * (threshold - data)$ ), a score that shows the disagreement between  
150 the expression data and the metabolic objective function. The normalised  
151 version of this score shows how well each gene in the expression data agrees  
152 with a particular metabolic function. GIMME has been successfully used in  
153 studies such as [41] aimed at understanding the impact of drought stress on  
154 *Arabidopsis thaliana*.

### 155 2.2.2. iMAT

156 The Integrative Metabolic Analysis Tool (iMAT) [42] takes three-valued  
157 expression data as inputs. The data are categorised as lowly, moderately, or

158 highly expressed and coded as -1, 0, and 1, respectively. A Boolean gene-to-  
159 reaction mapping is used to identify the state of a reaction, i.e., if the genes  
160 encoding enzymes of the reaction are low, moderate or highly expressed.  
161 This leads to classifying the reactions in the model as either highly or lowly  
162 expressed. This is followed by finding the steady state flux distribution that  
163 satisfies the stoichiometric and dynamic constraints and maximises the num-  
164 ber of reactions whose activity is consistent with their expression state. A  
165 reaction is considered active if it carries a significant positive flux (or negative  
166 flux for reversible reactions) that is greater than a threshold. A reaction is  
167 inactive if it carries a flux of zero (0). The algorithm returns a vector show-  
168 ing the predicted activity state (fluxes) of each reaction. iMAT performs  
169 a pathway enrichment analysis and identifies up- and down-regulated genes  
170 thus shedding light on the active pathways in the conditions under study.

### 171 2.2.3. FASTCORE

172 FASTCORE [43] is a data integration algorithm that accepts a core set of  
173 reactions that are known to be active in regard to the context under study.  
174 The core set of reactions can be determined by considering reactions in which  
175 highly expressed genes (genes whose expression level is above a predefined  
176 threshold) are involved. This is followed by a search for a flux consistent  
177 subnetwork, i.e., a network in which each reaction has a non zero flux in  
178 at least one feasible flux distribution. Such subnetwork presents a context-  
179 specific model which contains no blocked reactions.

### 180 2.2.4. INIT and tINIT

181 Intergrative Network Inference for Tissues (INIT) [44] formulates a mixed  
182 integer-linear problem (MILP) designed to use data from the Human Protein  
183 Atlas (HPA) and other omics data as inputs. INIT does not apply a strict  
184 steady state assumption for all internal metabolites. Instead it allows a small  
185 positive net production of metabolites which are given positive weights in the  
186 optimization. Consequently, all reactions in the resulting model are able to  
187 carry flux. The algorithm produces networks that are snapshots of active  
188 metabolism [45]. tINIT is the task-driven version of INIT. Here, a set of  
189 tasks that must be carried out by the resulting model are defined first and  
190 then followed by the INIT algorithm.

### 191 2.3. Case study using gene expression data from *Cyp51* knockout mice

192 The mouse gene expression dataset was downloaded from the GEO database  
193 (accession number GSE58271) and processed to obtain normalised gene ex-

194 pression values. Briefly, this dataset was generated from a study in which  
195 the mice were divided into three groups and fed on three diets i.e. low fat  
196 without cholesterol (LFnC), high fat without cholesterol (HFnC) and high fat  
197 with cholesterol (HFC). Each diet group contained both wild type and the  
198 *Cyp51* knockout genotype in female and male mice. The detailed description  
199 of the dataset can be found in [46].

200 Extraction of context-specific models was performed in Matlab R2019b  
201 (MathWorks Inc., Natick, Massachusetts, USA) using normalised gene ex-  
202 pression data and each of the model extraction methods (MEMs) above as  
203 described by their respective authors. A recently published mouse model,  
204 iMM1865 was used as a reference model. This model has 10612 reactions,  
205 5839 metabolites and 93 subsystems and has no dead-end metabolites or  
206 blocked reactions [47]. Highly expressed genes for model extraction were  
207 determined by setting the threshold values at the 50<sup>th</sup>, 70<sup>th</sup>, 75<sup>th</sup>, and 80<sup>th</sup>  
208 percentiles of the normalised gene expression data per sample. The rationale  
209 of setting this threshold per sample is that all individuals are biologically  
210 distinct even when under similar conditions. They yield unique expression  
211 patterns implying that their set of highly expressed genes may differ because  
212 of these intricate biological differences. Additionally, we assessed the impact  
213 of using thresholds set per each gene separately, i.e., thresholds defined within  
214 a gene. Here, we considered the 80<sup>th</sup>, 90<sup>th</sup>, 95<sup>th</sup> percentile and the mean for  
215 each gene within the observed population. The thresholds were chosen based  
216 on the trend of the variance explained by the first principal component (PC1)  
217 (Figure 1c and d). The extracted models from each algorithm were compared  
218 with one another (pairwise comparison) using the Jaccard index (distance)  
219 metric [48] to identify the distance between models extracted under the same  
220 conditions.

221 Principal component analysis (PCA) was performed as described in Op-  
222 dam et al. 2017 [16]. For every MEM, a matrix showing if a reaction was  
223 present (1) or absent (0) was generated. Reactions that were present or  
224 absent in all observed models were removed, and row means of the matrix  
225 were zero-centered. Principal component analysis on reactions was then per-  
226 formed. Furthermore, the variance explained by each factor (MEM, diet,  
227 gender, genotype) within a principal component was calculated by taking  
228 the square of the maximum Pearson correlation coefficient ( $R^2$ ) of the com-  
229 ponent scores across all possible orderings of the factors as described in [16].  
230 This was reported as a percentage. The validity of model separation observed  
231 in PCA was confirmed using t-distributed stochastic neighbour embedding

232 (t-SNE), which is particularly suitable for high-dimensional data [49].

233 To assess the dynamical response of the models, we performed flux sam-  
234 pling using the artificial centering hit-and-run (ACHR) algorithm [50] on the  
235 extracted models. 1000 flux samples were generated for each of the mod-  
236 els, and the mean flux of each reaction was used to identify the reactions  
237 that are either down- or up-regulated in pairwise comparisons of specific  
238 factors (diet, gender, and genotype) according to Spearman's rank correla-  
239 tion. The reactions identified to be significantly changed were then used  
240 to perform the enrichment analysis of metabolic subsystems using the hy-  
241 pergeometric test. The obtained p-values were adjusted for multiple test-  
242 ing using the Benjamini-Hochberg procedure. The implementation of the  
243 described analysis is available as a set of IPython (IPYNB) notebooks at  
244 [https://github.com/CompBioLj/GEMS\\_and\\_MEMS](https://github.com/CompBioLj/GEMS_and_MEMS).

### 245 3. Results

#### 246 3.1. Thresholds affect the extracted models

247 Our results indicate that the models extracted with the iMAT method-  
248 ology were able to explain the highest amount of variance in comparison to  
249 other model extraction methods (see Section 3.2 and Figure 2d). We thus  
250 opted to use the iMAT GEMs to assess the impact of thresholding on the  
251 extracted models. Two types of thresholds were used. First, thresholds were  
252 considered for each sample. This was done by taking a certain percentile of  
253 all the data within each sample to get the cutoff for highly expressed genes  
254 in that sample. This was achieved by taking a certain percentile of data to  
255 get the cutoff for highly expressed genes in that sample. The 50<sup>th</sup>, 70<sup>th</sup>, 75<sup>th</sup>  
256 and 80<sup>th</sup> percentile were considered. With the exception of models extracted  
257 at the 50<sup>th</sup> percentile threshold, the range and distribution of the Jaccard  
258 index and the size of the models were generally similar (see Figures 1a and  
259 b). The percentage of variance explained by the PC1 was the smallest at the  
260 50<sup>th</sup> percentile threshold but similar for other threshold values (see Figure  
261 1c).

262 The second type of thresholds was set per gene, i.e., by taking a percentile  
263 per gene for all samples. In this case the same threshold values were used  
264 for all samples, but were different among different genes. We considered the  
265 80<sup>th</sup>, 90<sup>th</sup> and 95<sup>th</sup> percentile gene expression for each gene as a cutoff to  
266 classify if a gene is highly expressed or not. We also considered taking the  
267 mean of each gene as a cutoff for the same purpose. From the perspective

268 of principal component analysis, the highest variance explained by PC1 was  
269 17% (see Figure 1d). Considering thresholds at 80<sup>th</sup>, 90<sup>th</sup> and 95<sup>th</sup> percentile,  
270 the highest variance explained by PC1 was achieved at the 90<sup>th</sup> percentile  
271 threshold.

272 PC1s from models where the threshold was taken per sample explained  
273 more variance than from models where the threshold was taken per gene.  
274 In general, the choice of thresholding strongly affected the content of the  
275 extracted models and their ability to capture variance in the data. Thresh-  
276 olding per sample with an 80<sup>th</sup> percentile as a cutoff value was considered as  
277 the most appropriate and was used in further analyses.

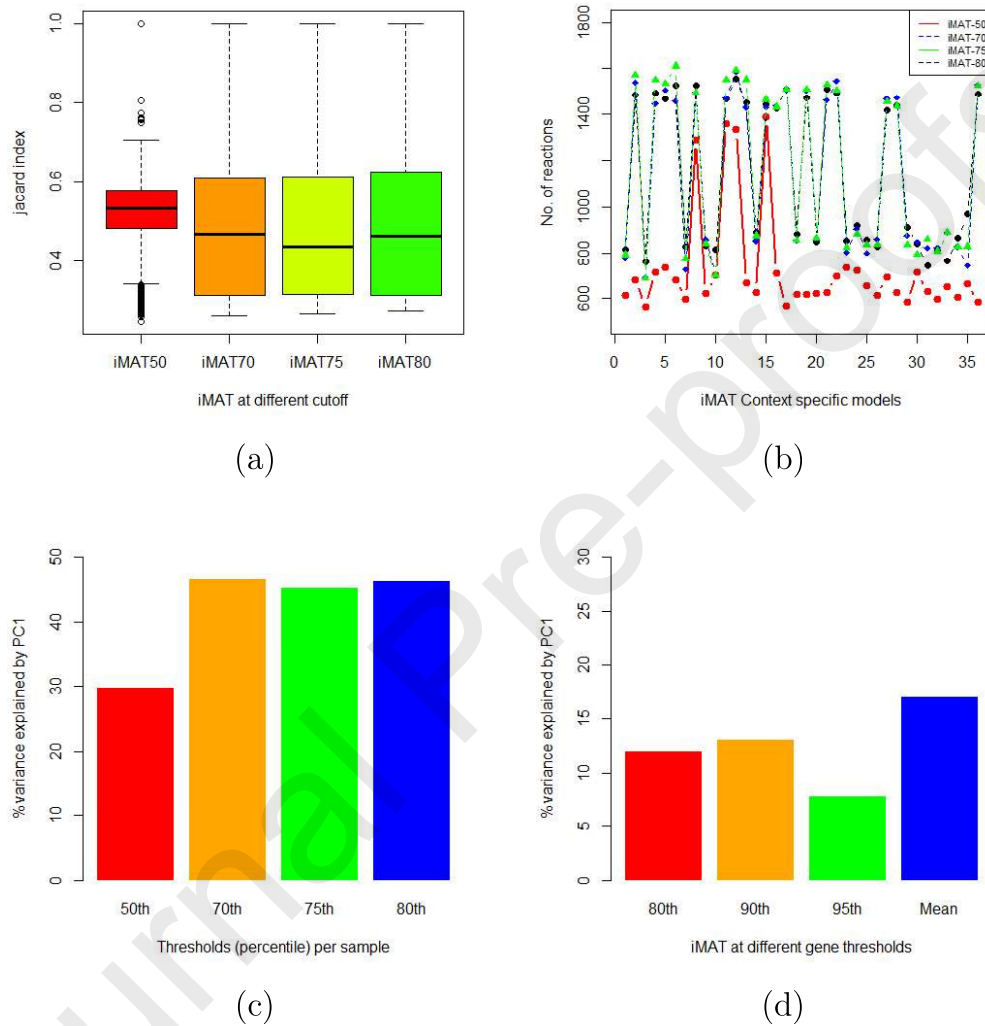


Figure 1: Analysis of iMAT derived models extracted using different thresholding rules and values. Figures 1 (a), (b), and (c) present the analysis of the models extracted by thresholding per sample, where figure (a) shows the Jaccard index from the pairwise comparisons of all models for each threshold, figure (b) how these models are varied in size, and figure (c) the percentage of variance explained by PC1 for each threshold. Figure (d) shows the variance explained by PC1 in the models extracted when thresholding is performed per gene. PC1: first principal component.

278 *3.2. Extracted models vary with algorithm*

279 Context-specific models were extracted using the GIMME, iMAT, FAST-  
280 CORE, INIT, and tINIT model extraction methods (MEMs). We performed  
281 the extraction process using the COBRA [51, 52] and RAVEN Toolboxes [53]  
282 in Matlab R2019b (MathWorks Inc., Natick, Massachusetts, USA) using the  
283 Gurobi solver [54].

284 The number of remaining reactions in an extracted model was considered  
285 to represent the size of a model. Different MEMs generated models of differ-  
286 ent sizes (see Figure 2a). iMAT-produced models were significantly different  
287 in size from other MEMs (t-test: p-value < 0.001). For each model within  
288 each MEM, we identified reactions that were present (1) or absent (0) and  
289 calculated the Jaccard index between all possible pairwise combinations to  
290 compare the similarities between models. For GIMME, FASTCORE, tINIT,  
291 and INIT, the Jaccard index was between 0.8 and 1.0, implying that these  
292 models are very similar (see Figure 2b). For iMAT, the Jaccard index ranged  
293 from 0.27 to 1.0, indicating that GEMs extracted with iMAT varied substan-  
294 tially (see Figures 2 b,c). Furthermore, we performed principal component  
295 analysis (PCA) on the matrix of reactions for each MEM. The PC1 explained  
296 the highest variance in iMAT derived models in comparison to PC1s of other  
297 MEMs (see Figure 2d).

298 In addition, we analysed how well do the clusters observed in the feature  
299 space described by the first two principal components (PC1 and PC2) comply  
300 with the groups defined by the experiment, namely diet, gender, and geno-  
301 type. The PCA plot (PC1 versus PC2) of models extracted with iMAT did  
302 not show consistent clustering of samples to predefined groups (see Supple-  
303 mentary Figure 1). This was similar for GIMME (see Supplementary Figure  
304 2). Separation by gender was consistent with the clustering by PC2 of INIT  
305 explaining approximately 8% of variance, and at least partially consistent  
306 with the clustering by PC2 of tINIT explaining approximately 7.4% of vari-  
307 ance in the data (see Supplementary Figures 3 and 4). GEMs extracted using  
308 FASTCORE were appropriately clustered by gender by the PC1 explaining  
309 approximately 13% of variance in the data (see Figure 3 and Supplementary  
310 Figure 5). All PCA plots performed on the FASTCORE extracted models  
311 are available as Supplementary Figure 5.

312 To verify the validity of the clustering obtained using PCA, we addition-  
313 ally performed t-distributed stochastic neighbour embedding (t-SNE) using  
314 different values of perplexity parameter [49]. Consistent clustering was ob-  
315 tained when the perplexity value was at least 15. The observed separation

316 of models complied with the PCA results (see Supplementary Figures 6 and  
317 7). Separation of models was consistent with gender in FASTCORE, INIT  
318 and tINIT, whereas using the PCA separation by gender was observed in  
319 FASTCORE and INIT and partially also in tINIT. Clustering by gender and  
320 only by gender was also observed in the original study [46], which confirms  
321 the adequacy of our analysis.

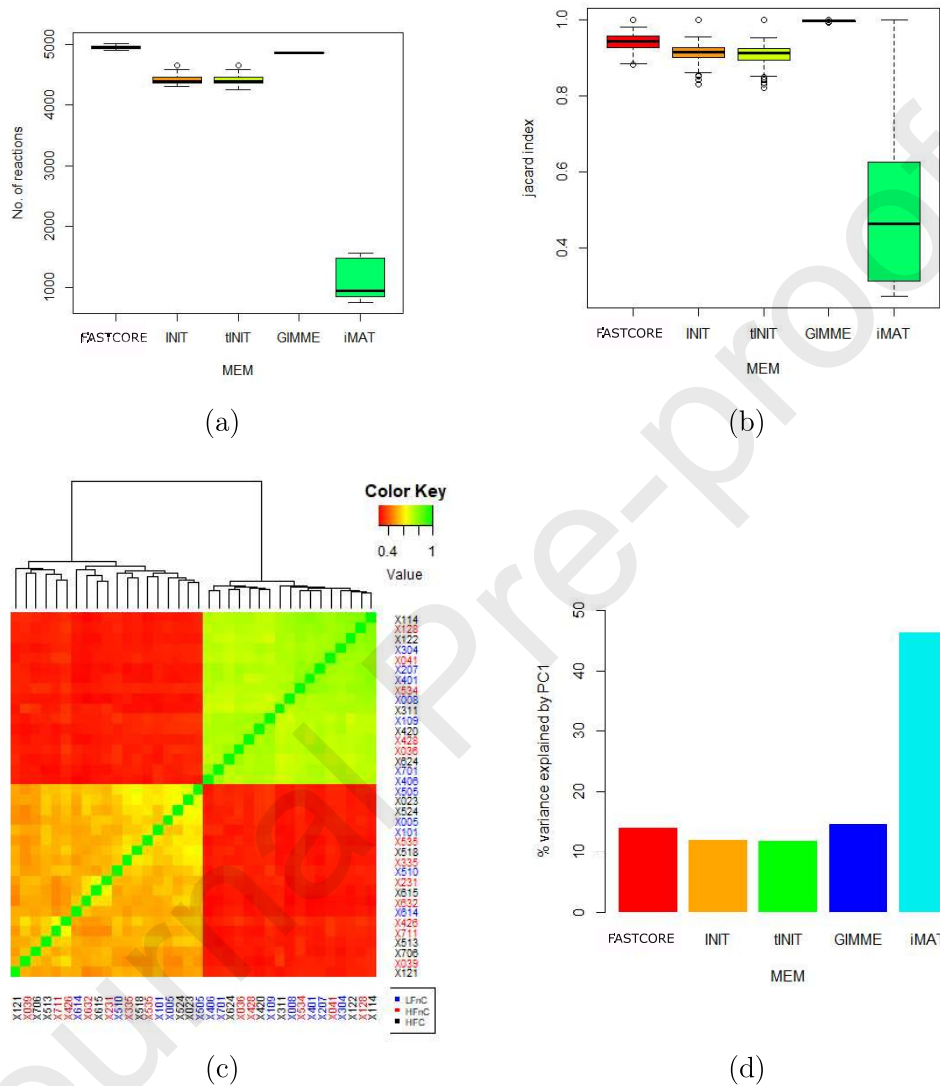


Figure 2: Comparison of models produced by different MEMs. Figure 2 (a) summarizes the size of the models, (b) summarizes the Jaccard indices, (c) shows the Jaccard indices of models produced by iMAT, and (d) shows the variance explained by PC1 of each MEM. PC1: first principal component; MEM: model extraction method.

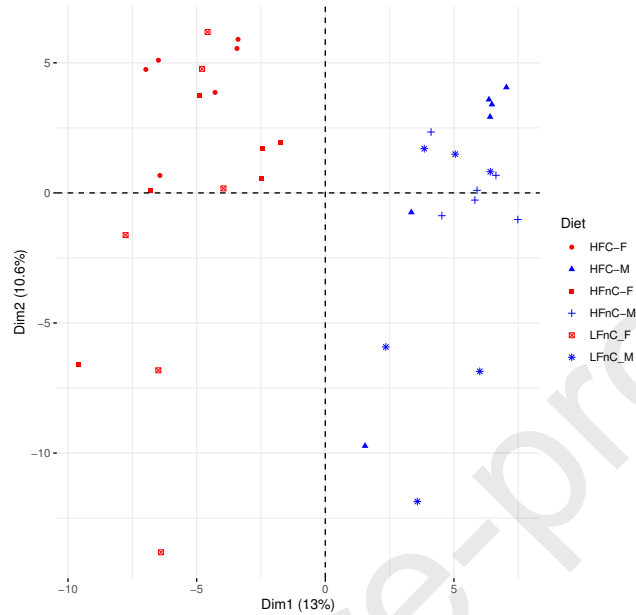
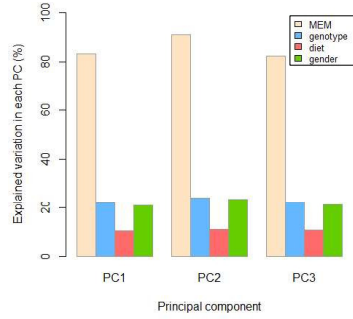
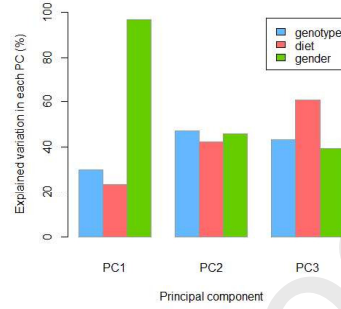


Figure 3: PCA plot showing separation by gender performed on the FASTCORE extracted models. Blue colour indicates male and red colour female samples, respectively. PCA: principal component analysis; F: female; M: male; LFnC: low fat without cholesterol; HFnC: high fat without cholesterol; HFC: high fat with cholesterol.

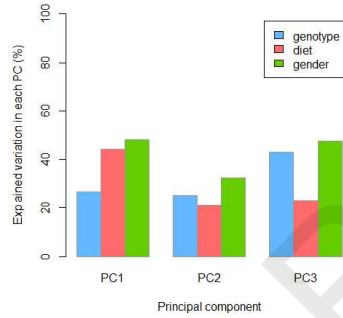
322 We further assessed how much each of the factors (MEM, diet, gender and  
 323 genotype) contributes to the variation explained by the first three principal  
 324 components (PCs). This was evaluated by taking each factor and calculating  
 325 the squares of Pearson correlation coefficient ( $R^2$ ) of component scores across  
 326 all possible orderings of the factors [16]. Considering all factors, the selection  
 327 of a MEM explains the most variability in the PCs (Figure 4a). Furthermore,  
 328 in FASTCORE (Figure 4b) and GIMME (Figure 4c) extracted models, gen-  
 329 der explained the most variability in the PCs as was also observed in the  
 330 original study [46].



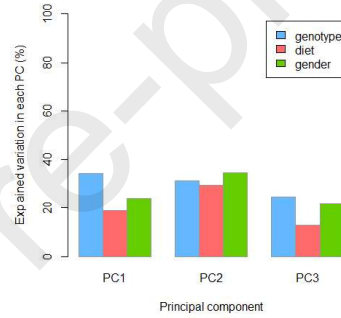
(a) All factors



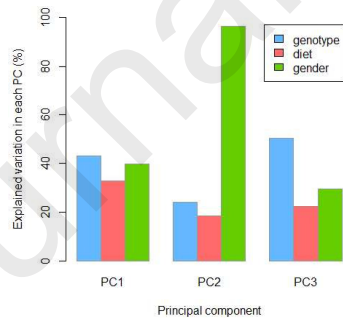
(b) FASTCORE



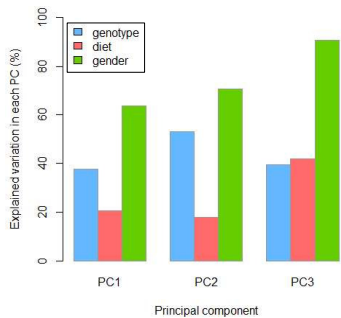
(c) GIMME



(d) iMAT



(e) INIT



(f) tINIT

Figure 4: Contribution of different factors, namely, MEM (yellow), diet (red), genotype (blue) and gender (green) to PC1, PC2 and PC3. Figure 4 (a) shows the contribution of all factors. Remaining figures show the contribution of diet, gender and genotype in models extracted with FASTCORE (b), GIMME (c), iMAT (d), INIT (e) and tINIT (f). MEM: model extraction method; PC: principal component.

331 In the models extracted with iMAT (Figure 4d), the observed three fac-  
332 tors, namely, gender, genotype, and diet, generally contributed equally with  
333 genotype having a slight edge in comparison to diet and gender. Gender ex-  
334 plained the most variability in models extracted with INIT and tINIT (Figure  
335 4e,f).

### 336 3.3. Enrichment analysis of metabolic subsystems

337 The models extracted with FASTCORE were able to capture the largest  
338 amount of true variability of the observed data (see Figure 3). We thus  
339 opted to perform further analysis only on these models. Since the basic  
340 version of flux balance analysis (FBA) is unable to provide unique solutions,  
341 we opted to analyse the activity of the observed metabolic reactions using flux  
342 sampling using the artificial centering hit-and-run (ACHR) algorithm [50].  
343 It was performed on the models extracted with the FASTCORE algorithm  
344 to obtain the mean values of reaction fluxes in each of the models. We  
345 performed the flux sampling using COBRA [51, 52] and the Gurobi solver  
346 [54] in Matlab R2019b.

347 We identified up- and down-regulated reactions between different groups  
348 of extracted models (e.g., wild type versus knockout groups) and their combi-  
349 nations using Spearman's rank correlation. Genome-scale metabolic models  
350 are usually composed of several subsystems containing metabolic reactions  
351 with a specific function (e.g. cholesterol synthesis subsystem) [52, 53]. Based  
352 on the identification of differentially regulated reactions, we further analysed  
353 the enriched subsystems between different groups using the hypergeometric  
354 test. We compared the models on the basis of diet (see Figure 5).

355 To check if the obtained models comply with our expectations, we further  
356 observed how different diets affect the cholesterol synthesis and metabolism  
357 subsystems. Figure 5 shows that cholesterol metabolism was enriched in  
358 mice on LFnC or HFnC diet compared to HFC diet. However, cholesterol  
359 metabolism was down-regulated in mice on LFnC diet compared to HFnC  
360 diet. Furthermore, Cholesterol synthesis was up-regulated in female wild  
361 type mice on LFnC diet compared to the HFC diet. In female knockout  
362 mice, cholesterol synthesis was down-regulated in mice on the LFnC diet in  
363 comparison to the mice on the HFnC diet. In wild type mice, cholesterol  
364 synthesis was up-regulated in mice on the HFnC diet compared to the HFC  
365 diet. There was no significant subsystem enrichment due to genotype or  
366 gender alone. A 5% level of significance after the adjustment for multiple  
367 testing (p-value:  $< 0.05$ ) was considered in all analyses.

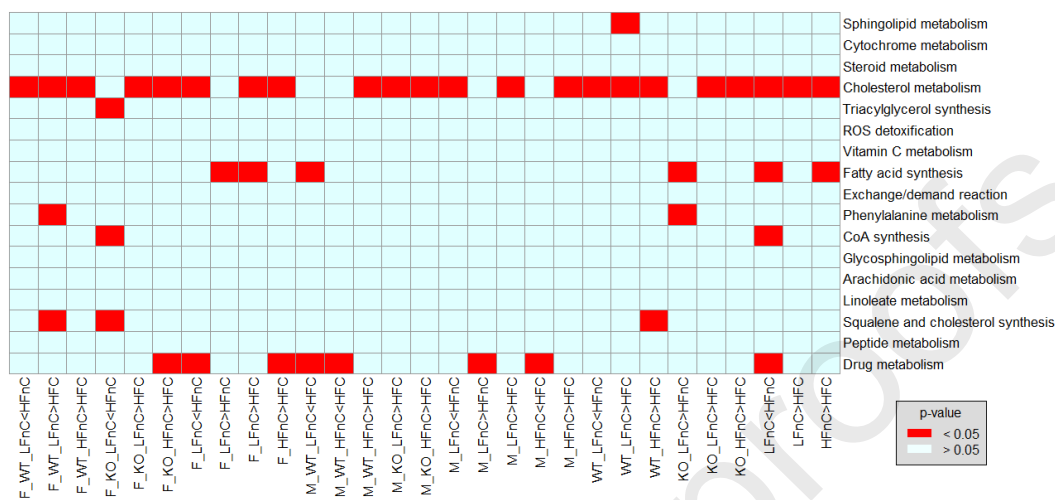


Figure 5: Metabolic subsystems enrichment analysis between different diets. Subsystems that were differentially enriched between two groups and those associated with cholesterol are shown. Cholesterol metabolism was enriched in mice on HFnC diet compared to HFC diet. The less than symbol (<) between the groups corresponds to down-regulation and the more than symbol (>) corresponds to up-regulation. F: female; M: male; WT: wild type; KO: knockout; LFnC: low fat without cholesterol; HFnC: high fat without cholesterol; HFC: high fat with cholesterol.

#### 368 4. Discussion

369 The aim of this work was to highlight the factors that have the strongest  
 370 influence on the context-specific extraction of genome-scale metabolic mod-  
 371 els, especially in relation to the model-based analysis of omics data. Addi-  
 372 tionally, we proposed a methodology that could be followed in such analyses  
 373 (see Figure 6). This is composed of the following steps: (1) identification of  
 374 the most suitable reference model; (2) extraction of context-specific GEMs  
 375 using different MEMs with different configurations; (3) identification of the  
 376 MEM and its configuration that is able to capture the variance of the ob-  
 377 served data as well as the groups defined in the experiment; (4) analysis  
 378 of obtained models using different approaches, such as PCA, t-SNE, and  
 379 metabolic subsystems enrichment analysis.

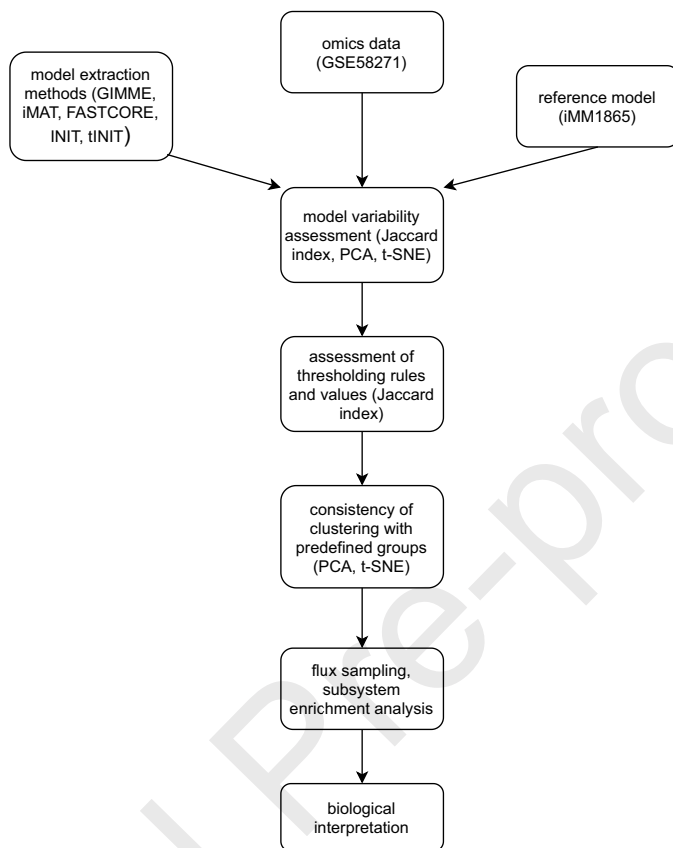


Figure 6: Overview of the proposed methodology. PCA: principal component analysis; t-SNE: t-distributed stochastic neighbour embedding.

380 We extracted GEMs using five model extraction methods i.e. GIMME,  
 381 iMAT, FASTCORE, INIT and tINIT. The results show that the choice of a  
 382 MEM affects the structure and contents of the output models. Additionally,  
 383 the models varied greatly in size between MEMs. INIT and tINIT are very  
 384 similar algorithms and so are their output models. These results are consis-  
 385 tent with published reports [16, 18, 17]. We used Jaccard index to assess how  
 386 much the models differed within each MEM and PCA to assess how much  
 387 variance in the data each MEM was able to capture. GIMME produced very  
 388 similar models and captured the least variability in the data. iMAT captured  
 389 the most variability in the data (46% by PC1) but was unable to capture  
 390 the true variability in the experiment. However, FASTCORE with 13% of  
 391 variance explained by PC1 in this example was able to capture the largest

392 amount of variability due to any of the observed factors, namely gender. Sim-  
393 ilar clustering was also observed in the original study [46]. This implies that  
394 it is important to select a MEM that not only captures the largest variance  
395 in the data, but also captures the groups that are aligned with predefined  
396 experimental groups. These groups could reflect different metabolic signa-  
397 tures and thus have a potential to guide downstream analyses. Our findings  
398 assert that the choice of a MEM greatly affects the output models.

399 We further assessed the impact of using different thresholds on the out-  
400 put models. Thresholds were set on gene expression data to identify highly  
401 expressed genes. For each model extracted with iMAT, we applied two kinds  
402 of thresholding, i.e., within a sample and within a gene. Thresholding within  
403 a sample captured unique individual differences in expression even if indi-  
404 viduals were from the same experimental group. We see that the type of  
405 thresholding applied and the threshold values used strongly affect the out-  
406 put models.

407 We performed subsystem enrichment analysis to assess how cholesterol  
408 metabolism and synthesis varied between the groups separated by different  
409 diets. This is because knocking out the *Cyp51* gene interrupts cholesterol  
410 synthesis and metabolism [46, 55, 56, 57]. In our analysis, models extracted  
411 with FASTCORE showed that cholesterol metabolism significantly changed  
412 between groups with different diets. Cholesterol metabolism was enriched in  
413 mice on LFnC or HFnC diet compared to HFC diet. However, cholesterol  
414 metabolism was down-regulated in mice on LFnC diet compared to HFnC  
415 diet.

416 The proposed methodology, like other analyses using GEMs, requires se-  
417 lection of a suitable reference model. The choice of a reference model strongly  
418 affects the output models. The model should optimally describe the same  
419 tissue or at least the same organism as the samples used in the experiment.  
420 Moreover, the model should contain accurate gene-product-reaction (GPR)  
421 rules, which are used by MEMs to connect the omics data with metabolic  
422 reactions. In our case, we used the most recently published mouse model,  
423 namely iMM1865 [47].

424 Different MEMs implement different algorithms for data integration. As  
425 such, the output models differ greatly in their contents. In this analysis,  
426 we opted to use a selection of the state-of-the-art MEMs, namely, GIMME,  
427 iMAT, FASTCORE, INIT, and tINIT. However, other algorithms, such as  
428 CORDA [58], mCADRE [59] and MBA [60] could as well be applied. Selected  
429 MEMs also need to be configured as required by a particular algorithm, e.g.,

430 with the identification of the most suitable thresholding rules and values. The  
431 choice of values for a particular configuration needs to be guided by known  
432 knowledge and further analyses performed on selected MEMs. Identification  
433 of the most suitable MEM(s) needs to be based on the results from the anal-  
434 ysis of the obtained models using different approaches, such as PCA, t-SNE,  
435 various distance metrics, and metabolic subsystem enrichment analysis. Ide-  
436 ally, a MEM of choice will explain the most variance in the observed dataset  
437 and will be able to separate the models in compliance with the groups defined  
438 in the experiment. Moreover, the obtained results of further analyses of the  
439 models extracted with the selected MEM will reflect the biological relevance  
440 and will provide a platform to generate novel knowledge and hypotheses.  
441 Such an ideal situation may not be obtained easily. When compromises are  
442 required, the MEM that best captures the groups defined by the experiment  
443 should be selected. In this context, the MEM that has the largest percentage  
444 of explained variance within the PC1 for a selected group should be selected  
445 (see Figure 4).

446 Even though the proposed methodology was demonstrated using only  
447 transcriptomics data, different omics data could as well be used in the pro-  
448 cess. For example, metabolomics and lipidomics data can be mapped into  
449 the context of metabolic reactions [61]. These can be used to identify a set  
450 of tasks or core reactions that need to be executed by a model. Moreover,  
451 specific model extraction methods, such as tINIT, allow a direct integra-  
452 tion of non-transcriptomics data. Namely, tINIT algorithm accepts a list of  
453 metabolites the model should be able to produce [45].

454 We propose that the analysis of omics data using GEMs should be ini-  
455 tiated with an extraction of different context-specific models using different  
456 MEMs. This should be followed with the application of various thresholding  
457 rules and different threshold values in the process of reconstruction. The  
458 resulting models should then be analysed to select the most appropriate  
459 MEM(s), threshold values and thresholding rules that best capture the vari-  
460 ability in the data while capturing the known experimental groups.

## 461 **Competing interests**

462 The authors declare that they have no competing interests.

463 **Authors' contributions**

464 **Andrew Walakira:** Methodology, Software, Formal analysis, Investiga-  
 465 tion, Writing – Original Draft, Writing – Review & Editing, Visualization  
 466 **Damjana Rozman:** Conceptualization, Writing – Review, Funding acqui-  
 467 sition & Editing **Tadeja Režen:** Conceptualization, Writing – Review &  
 468 Editing **Miha Mraz:** Writing – Review & Editing, Funding acquisition, Su-  
 469 pervision **Miha Moškon:** Conceptualization, Methodology, Software, For-  
 470 mal analysis, Investigation, Writing – Review & Editing, Supervision

471 **Acknowledgements**

472 This work was supported by the Horizon 2020 TranSYS Marie Curie  
 473 Initial Training Network Grant Agreement No. 860895, by the scientific re-  
 474 search programs Pervasive Computing (P2-0359) and Functional Genomics  
 475 and Biotechnology for Health (P1-0390) both financed by the Slovenian Re-  
 476 search Agency, and by the basic research project CholesteROR in metabolic  
 477 liver diseases (J1-9176) financed by the Slovenian Research Agency. We  
 478 would like to acknowledge John Hancock for proofreading the manuscript.

479 **References**

- 480 [1] R. Wang, B. Li, S. M. Lam, G. Shui, Integration of lipidomics and  
 481 metabolomics for in-depth understanding of cellular mechanism and dis-  
 482 ease progression, *Journal of Genetics and Genomics* 47 (2) (2020) 69–83.
- 483 [2] A. Faulkner, Z. Dang, E. Avolio, A. C. Thomas, T. Batstone, G. R.  
 484 Lloyd, R. J. Weber, L. Najdekr, A. Jankevics, W. B. Dunn, et al.,  
 485 Multi-omics analysis of diabetic heart disease in the db/db model reveals  
 486 potential targets for treatment by a longevity-associated gene, *Cells* 9 (5)  
 487 (2020) 1283.
- 488 [3] O. Ivanova, L. B. Richards, S. J. Vijverberg, A. H. Neerincx, A. Sinha,  
 489 P. J. Sterk, A. H. Maitland-van der Zee, What did we learn from multiple  
 490 omics studies in asthma?, *Allergy* 74 (11) (2019) 2129–2145.
- 491 [4] H.-G. Hwang, K.-J. Kim, S.-H. Lee, C.-K. Kim, C.-K. Min, J.-M. Yun,  
 492 S. U. Lee, Y.-J. Son, et al., Recombinant glargine insulin production  
 493 process using escherichia coli, *J Microbiol Biotechnol* 26 (10) (2016)  
 494 1781–9.

- 495 [5] K. Govender, T. Naicker, J. Lin, S. Baijnath, A. A. Chuturgoon, N. S.  
496 Abdul, T. Docrat, H. G. Kruger, T. Govender, A novel and more efficient  
497 biosynthesis approach for human insulin production in escherichia coli  
498 (e. coli), *AMB Express* 10 (1) (2020) 1–9.
- 499 [6] M. R. Pulido, M. García-Quintanilla, M. L. Gil-Marqués, M. J. Mc-  
500 Connell, Identifying targets for antibiotic development using omics tech-  
501 nologies, *Drug discovery today* 21 (3) (2016) 465–472.
- 502 [7] O. S. Mohite, T. Weber, H. U. Kim, S. Y. Lee, Genome-scale metabolic  
503 reconstruction of actinomycetes for antibiotics production, *Biotechnol-  
504 ogy Journal* 14 (1) (2019) 1800377.
- 505 [8] K. Siren, Multi-omics methods to unravel microbial diversity in fer-  
506 mentation of riesling wines, Ph.D. thesis, TU Kaiserslautern, Germany  
507 (2019).
- 508 [9] Z. Mirzoyan, M. Sollazzo, M. Allocca, A. M. Valenza, D. Grifoni, P. Bel-  
509 losta, *Drosophila melanogaster*: A model organism to study cancer,  
510 *Frontiers in Genetics* 10 (2019) 51.
- 511 [10] Y. Xiong, J. Yu, Modeling parkinson’s disease in drosophila: what have  
512 we learned for dominant traits?, *Frontiers in Neurology* 9 (2018) 228.
- 513 [11] B. Ugur, K. Chen, H. J. Bellen, *Drosophila* tools and assays for the  
514 study of human diseases, *Disease models & mechanisms* 9 (3) (2016)  
515 235–244.
- 516 [12] C. Gu, G. B. Kim, W. J. Kim, H. U. Kim, S. Y. Lee, Current status and  
517 applications of genome-scale metabolic models, *Genome biology* 20 (1)  
518 (2019) 1–18.
- 519 [13] K. Blagotinšek Cokan, Ž. Urlep, M. Moškon, M. Mraz, X. Y. Kong,  
520 W. Eskild, D. Rozman, P. Juvan, T. Režen, Common transcriptional  
521 program of liver fibrosis in mouse genetic models and humans, *Internation-  
522 al Journal of Molecular Sciences* 22 (2) (2021) 832.
- 523 [14] W. M. Schneider, J. M. Luna, H.-H. Hoffmann, F. J. Sánchez-Rivera,  
524 A. A. Leal, A. W. Ashbrook, J. Le Pen, I. Ricardo-Lax, E. Michailidis,  
525 A. Peace, et al., Genome-scale identification of SARS-CoV-2 and pan-  
526 coronavirus host factor networks, *Cell* 184 (1) (2021) 120–132.

- 527 [15] H. Hozhabri, A. Lashkari, S.-M. Razavi, A. Mohammadian, Integration  
528 of gene expression data identifies key genes and pathways in colorectal  
529 cancer, *Medical Oncology* 38 (1) (2021) 1–14.
- 530 [16] S. Opdam, A. Richelle, B. Kellman, S. Li, D. C. Zielinski, N. E. Lewis,  
531 A systematic evaluation of methods for tailoring genome-scale metabolic  
532 models, *Cell systems* 4 (3) (2017) 318–329.
- 533 [17] A. Richelle, C. Joshi, N. E. Lewis, Assessing key decisions for transcrip-  
534 tomic data integration in biochemical networks, *PLoS computational  
535 biology* 15 (7) (2019) e1007185.
- 536 [18] A. Richelle, A. W. Chiang, C.-C. Kuo, N. E. Lewis, Increasing consensus  
537 of context-specific metabolic models by integrating data-inferred cell  
538 functions, *PLoS computational biology* 15 (4) (2019) e1006867.
- 539 [19] A. M. Feist, M. J. Herrgård, I. Thiele, J. L. Reed, B. Ø. Palsson, Recon-  
540 struction of biochemical networks in microorganisms, *Nature Reviews  
541 Microbiology* 7 (2) (2009) 129–143.
- 542 [20] Z. Hosseini, S.-A. Marashi, Discovering missing reactions of metabolic  
543 networks by using gene co-expression data, *Scientific reports* 7 (1) (2017)  
544 1–12.
- 545 [21] I. Thiele, N. Vlassis, R. M. Fleming, fastgapfill: efficient gap filling in  
546 metabolic networks, *Bioinformatics* 30 (17) (2014) 2529–2531.
- 547 [22] J. P. Brooks, W. P. Burns, S. S. Fong, C. M. Gowen, S. B. Roberts,  
548 Gap detection for genome-scale constraint-based models, *Advances in  
549 bioinformatics* 2012 (2012).
- 550 [23] C. S. Jensen, C. J. Norsigian, X. Fang, X. C. Nielsen, J. J. Christensen,  
551 B. O. Palsson, J. M. Monk, Reconstruction and validation of a genome-  
552 scale metabolic model of streptococcus oralis (iCJ415), a human com-  
553 mensal and opportunistic pathogen, *Frontiers in genetics* 11 (2020) 116.
- 554 [24] L. de Arroyo Garcia, P. R. Jones, In silico co-factor balance estima-  
555 tion using constraint-based modelling informs metabolic engineering in  
556 *escherichia coli*, *PLoS computational biology* 16 (8) (2020) e1008125.

- 557 [25] J. L. Reed, Genome-scale metabolic modeling and its application to  
558 microbial communities, in: *The Chemistry of Microbiomes: Proceedings*  
559 *of a Seminar Series*, National Academies Press (US), 2017, pp. 85–92.
- 560 [26] J. D. Orth, I. Thiele, B. Ø. Palsson, What is flux balance analysis?,  
561 *Nature biotechnology* 28 (3) (2010) 245–248.
- 562 [27] S. Volkova, M. R. Matos, M. Mattanovich, I. Marín de Mas, Metabolic  
563 modelling as a framework for metabolomics data integration and anal-  
564 ysis, *Metabolites* 10 (8) (2020) 303.
- 565 [28] M. Lularevic, A. J. Racher, C. Jaques, A. Kiparissides, Improving the  
566 accuracy of flux balance analysis through the implementation of car-  
567 bon availability constraints for intracellular reactions, *Biotechnology and*  
568 *bioengineering* 116 (9) (2019) 2339–2352.
- 569 [29] J.-C. Lachance, C. J. Lloyd, J. M. Monk, L. Yang, A. V. Sastry, Y. Seif,  
570 B. O. Palsson, S. Rodrigue, A. M. Feist, Z. A. King, et al., Bofdat:  
571 Generating biomass objective functions for genome-scale metabolic mod-  
572 els from experimental data, *PLoS computational biology* 15 (4) (2019)  
573 e1006971.
- 574 [30] M. Budinich, J. Bourdon, A. Larhlimi, D. Eveillard, A multi-objective  
575 constraint-based approach for modeling genome-scale microbial ecosys-  
576 tems, *PloS one* 12 (2) (2017) e0171744.
- 577 [31] A. Patané, G. Jansen, P. Conca, G. Carapezza, J. Costanza, G. Nicosia,  
578 Multi-objective optimization of genome-scale metabolic models: the case  
579 of ethanol production, *Annals of Operations Research* 276 (1-2) (2019)  
580 211–227.
- 581 [32] J. S. Edwards, B. O. Palsson, Metabolic flux balance analysis and the  
582 in silico analysis of *Escherichia coli* K-12 gene deletions, *BMC bioinfor-*  
583 *matics* 1 (1) (2000) 1–10.
- 584 [33] N. E. Lewis, K. K. Hixson, T. M. Conrad, J. A. Lerman, P. Charusanti,  
585 A. D. Polpitiya, J. N. Adkins, G. Schramm, S. O. Purvine, D. Lopez-  
586 Ferrer, et al., Omic data from evolved *E. coli* are consistent with com-  
587 puted optimal growth from genome-scale models, *Molecular systems bi-*  
588 *ology* 6 (1) (2010) 390.

- 589 [34] S. Gudmundsson, I. Thiele, Computationally efficient flux variability  
590 analysis, *BMC bioinformatics* 11 (1) (2010) 1–3.
- 591 [35] N. E. Lewis, H. Nagarajan, B. O. Palsson, Constraining the metabolic  
592 genotype–phenotype relationship using a phylogeny of in silico methods,  
593 *Nature Reviews Microbiology* 10 (4) (2012) 291–305.
- 594 [36] W. Megchelenbrink, M. Huynen, E. Marchiori, optgpsampler: an im-  
595 proved tool for uniformly sampling the solution-space of genome-scale  
596 metabolic networks, *PloS one* 9 (2) (2014) e86587.
- 597 [37] H. A. Herrmann, B. C. Dyson, L. Vass, G. N. Johnson, J.-M. Schwartz,  
598 Flux sampling is a powerful tool to study metabolism under changing  
599 environmental conditions, *NPJ systems biology and applications* 5 (1)  
600 (2019) 1–8.
- 601 [38] S. Robaina Estévez, Z. Nikoloski, Generalized framework for context-  
602 specific metabolic model extraction methods, *Frontiers in plant science*  
603 5 (2014) 491.
- 604 [39] S. A. Becker, B. O. Palsson, Context-specific metabolic networks are  
605 consistent with experiments, *PLoS Comput Biol* 4 (5) (2008) e1000082.
- 606 [40] M. K. Kim, D. S. Lun, Methods for integration of transcriptomic data in  
607 genome-scale metabolic models, *Computational and structural biotech-  
608 nology journal* 11 (18) (2014) 59–65.
- 609 [41] R. Siritwach, F. Matsuda, K. Yano, M. Y. Hirai, Drought stress re-  
610 sponses in context-specific genome-scale metabolic models of *arabidopsis  
611 thaliana*, *Metabolites* 10 (4) (2020) 159.
- 612 [42] H. Zur, E. Ruppin, T. Shlomi, iMAT: an integrative metabolic analysis  
613 tool, *Bioinformatics* 26 (24) (2010) 3140–3142.
- 614 [43] N. Vlassis, M. P. Pacheco, T. Sauter, Fast reconstruction of compact  
615 context-specific metabolic network models, *PLoS Comput Biol* 10 (1)  
616 (2014) e1003424.
- 617 [44] R. Agren, S. Bordel, A. Mardinoglu, N. Pornputtpong, I. Nookaew,  
618 J. Nielsen, Reconstruction of genome-scale active metabolic networks  
619 for 69 human cell types and 16 cancer types using INIT, *PLoS Comput  
620 Biol* 8 (5) (2012) e1002518.

- 621 [45] R. Agren, A. Mardinoglu, A. Asplund, C. Kampf, M. Uhlen, J. Nielsen,  
622 Identification of anticancer drugs for hepatocellular carcinoma through  
623 personalized genome-scale metabolic modeling, *Molecular systems biol-*  
624 *ogy* 10 (3) (2014) 721.
- 625 [46] G. Lorbek, M. Perše, J. Jeruc, P. Juvan, F. M. Gutierrez-Mariscal,  
626 M. Lewinska, R. Gebhardt, S. Horvat, I. Björkhem, D. Rozman, et al.,  
627 Lessons from hepatocyte-specific Cyp51 knockout mice: impaired choles-  
628 terol synthesis leads to oval cell-driven liver injury, *Scientific reports* 5 (1)  
629 (2015) 1–11.
- 630 [47] S. Khodae, Y. Asgari, M. Totonchi, M. H. Karimi-Jafari, imm1865: A  
631 new reconstruction of mouse genome-scale metabolic model, *Scientific*  
632 *reports* 10 (1) (2020) 1–13.
- 633 [48] N. C. Chung, B. Miasojedow, M. Startek, A. Gambin, Jac-  
634 card/Tanimoto similarity test and estimation methods for biological  
635 presence-absence data, *BMC bioinformatics* 20 (15) (2019) 1–11.
- 636 [49] L. Van der Maaten, G. Hinton, Visualizing data using t-SNE., *Journal*  
637 *of machine learning research* 9 (11) (2008).
- 638 [50] S. Fallahi, H. J. Skaug, G. Alendal, A comparison of monte carlo sam-  
639 pling methods for metabolic network models, *Plos one* 15 (7) (2020)  
640 e0235393.
- 641 [51] S. A. Becker, A. M. Feist, M. L. Mo, G. Hannum, B. Ø. Palsson,  
642 M. J. Herrgard, Quantitative prediction of cellular metabolism with  
643 constraint-based models: the cobra toolbox, *Nature protocols* 2 (3)  
644 (2007) 727–738.
- 645 [52] L. Heirendt, S. Arreckx, T. Pfau, S. N. Mendoza, A. Richelle,  
646 A. Heinken, H. S. Haraldsdóttir, J. Wachowiak, S. M. Keating,  
647 V. Vlasov, et al., Creation and analysis of biochemical constraint-based  
648 models using the cobra toolbox v. 3.0, *Nature protocols* 14 (3) (2019)  
649 639–702.
- 650 [53] H. Wang, S. Marcišauskas, B. J. Sánchez, I. Domenzain, D. Hermansson,  
651 R. Agren, J. Nielsen, E. J. Kerkhoven, Raven 2.0: A versatile toolbox  
652 for metabolic network reconstruction and a case study on streptomyces  
653 coelicolor, *PLoS computational biology* 14 (10) (2018) e1006541.

- 654 [54] L. Gurobi Optimization, Gurobi optimizer reference manual (2021).  
655 URL <http://www.gurobi.com>
- 656 [55] Ž. Urlep, G. Lorbek, M. Perše, J. Jeruc, P. Juvan, M. Matz-Soja, R. Geb-  
657 hardt, I. Björkhem, J. A. Hall, R. Bonneau, et al., Disrupting hepatocyte  
658 Cyp51 from cholesterol synthesis leads to progressive liver injury in the  
659 developing mouse and decreases rorc signalling, *Scientific reports* 7 (1)  
660 (2017) 1–13.
- 661 [56] K. B. Cokan, Ž. Urlep, G. Lorbek, M. Matz-Soja, C. Skubic, M. Perše,  
662 J. Jeruc, P. Juvan, T. Režen, D. Rozman, Chronic disruption of the  
663 late cholesterol synthesis leads to female-prevalent liver cancer, *Cancers*  
664 12 (11) (2020) 3302.
- 665 [57] C. Skubic, D. Rozman, Sterols from the post-lanosterol part of choles-  
666 terol synthesis: Novel signaling players, in: *Mammalian Sterols*,  
667 Springer, 2020, pp. 1–22.
- 668 [58] A. Schultz, A. A. Qutub, Reconstruction of tissue-specific metabolic  
669 networks using CORDA, *PLoS computational biology* 12 (3) (2016)  
670 e1004808.
- 671 [59] Y. Wang, J. A. Eddy, N. D. Price, Reconstruction of genome-scale  
672 metabolic models for 126 human tissues using mCADRE, *BMC systems*  
673 *biology* 6 (1) (2012) 153.
- 674 [60] L. Jerby, T. Shlomi, E. Ruppin, Computational reconstruction of tissue-  
675 specific metabolic models: application to human liver metabolism,  
676 *Molecular systems biology* 6 (1) (2010) 401.
- 677 [61] N. Poupin, F. Vinson, A. Moreau, A. Batut, M. Chazalviel, B. Colsch,  
678 L. Fouillen, S. Guez, S. Khoury, J. Dalloux-Chioccioli, et al., Improv-  
679 ing lipid mapping in genome scale metabolic networks using ontologies,  
680 *Metabolomics* 16 (4) (2020) 1–11.